Supporting Information

Nitrogen-doped polymer nanofibers decorated with Co nanoparticles for uniform lithium nucleation/growth in lithium metal batteries

Miao Shu, Xing Li*, Liqiang Duan, Mengting Zhu, Xing Xin*

School of Material Science and Chemical Engineering, Ningbo University, Key Laboratory of Photoelectric Materials and Devices of Zhejiang Province, Ningbo, 315211, China

* E-mail: lixing@nbu.edu.cn

* E-mail: xinxing@nbu.edu.cn

Supplementary Index

Fig. S5 XPS spectra of the Co/CNFs-750: (a) N1s spectrum, and (b) C1s spectrum, and (c) O1s spectrum, and (d) Co2p spectrum.

Fig. S6 (a) Raman spectra, and (b) XRD spectra of the Co/CNFs in different calcination temperature at 450 ℃, 550 ℃, 650 ℃, 750 ℃, repectively. (c) The FTIR spectrum: the spectra of the Co/CNFs in the calcination temperature at 450 ℃ a, 550 ℃ b, 650 ℃ c, 750 ℃ d, the spectra of pure PAN fibers before calcination e, the spectra of pure PAN fibers after calcination f. (d) TG spectra of the purple ZIF-67 crystals on PAN NFs film at N_2 atmosphere.

Fig. S7 The weight loss rate of the Co/CNFs in O_2 atmosphere in different calcination temperature at (a) 450 ℃, and (b) 550 ℃, and (c) 650 ℃, and (d) 750 ℃, respectively.

Fig. S8 Voltage profiles of metallic Li plating/stripping in five styles of symmetric cells (Li/Co/CNFs-750 modified Li, Li/Co/CNFs-650 modified Li, Li/Co/CNFs-550 modified Li, Li/Co/CNFs-450 modified Li and Li/Li) at the current density of 1.0 mA cm^{-2} with the capacity limit of 0.5 mAh cm^{-2}.

Fig. S9 Voltage profiles of metallic Li plating/stripping in symmetric cells of Li/Co/CNFs-750 modified Li at different current densities of 0.5 mA cm^{-2}, 1.0 mA cm^{-2}, 1.5 mA cm^{-2} with the capacity limit of 0.5 mAh cm^{-2} and its expanded view from 170 to 180 h.

Fig. S10 (a,b) Surface SEM images of the Co/CNFs-750 modified Li electrode at the lithiation capacity of 15 mAh cm^{-2} (30h).

Fig. S11 (a,b) Surface SEM images of the bare Li-metal electrode, and (c,d) the Co/CNFs-750 interlayer before Li deposition.

Fig. S12 (a,d) The surface SEM morphologies of the Co/CNFs-750 interlayer facing the separator, and (b,e) the Co/CNFs-750 interlayer backing the separator, and (c,f) the cross-section SEM images of the Co/CNFs-750 interlayer at the different lithiation capacities of 5 mAh cm^{-2} (10 h) and 10 mAh cm^{-2} (20h), respectively.

Fig. S13 SEM image of the Co/CNFs interlayers before cycling.

Fig. S14 The coulombic efficiencies of the full cells with three style electrodes at 1.0 C.

Fig. S15 (a) Cycling performance of the full cells at 2.0 C. (b) The charge/discharge profiles of full cells with $LiFePO_4$ as the cathode and the Co/CNFs-750 modified Li as the anode at 2.0 C.

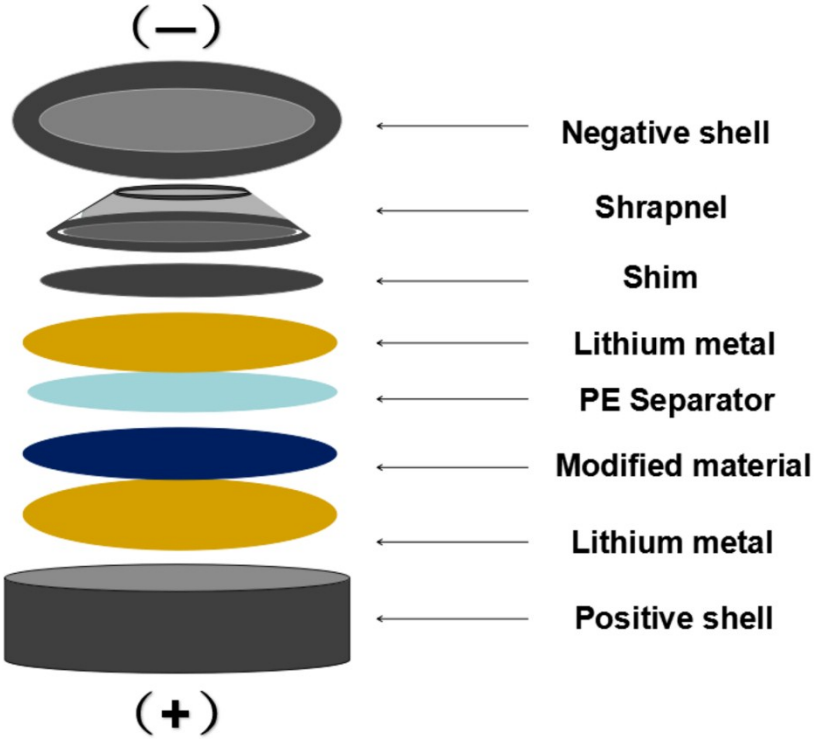

Fig. S1 Schematic diagram of the assembly of each part in the battery.

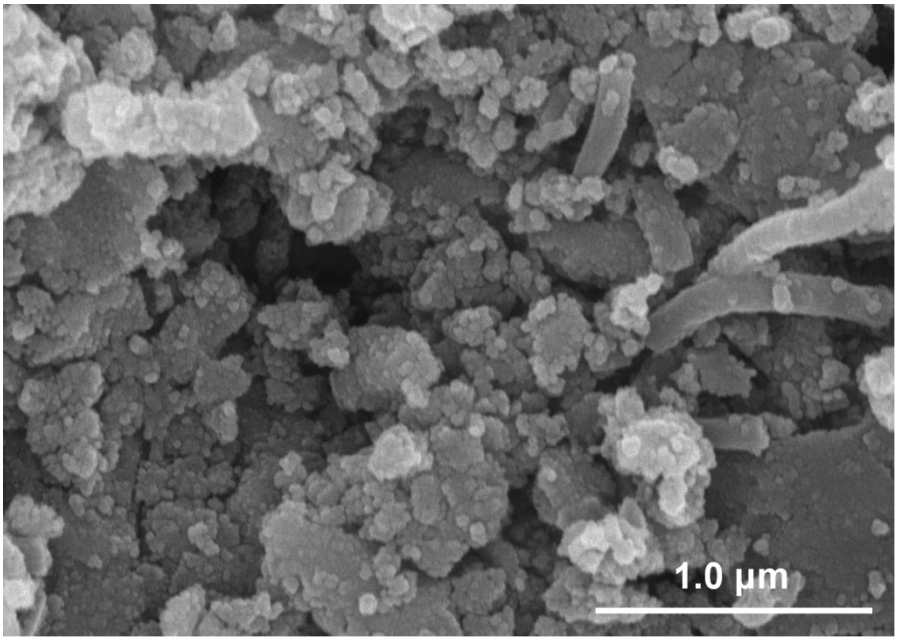

Fig. S2 SEM image of the Co/CNFs interlayers sintering at 850 ℃.

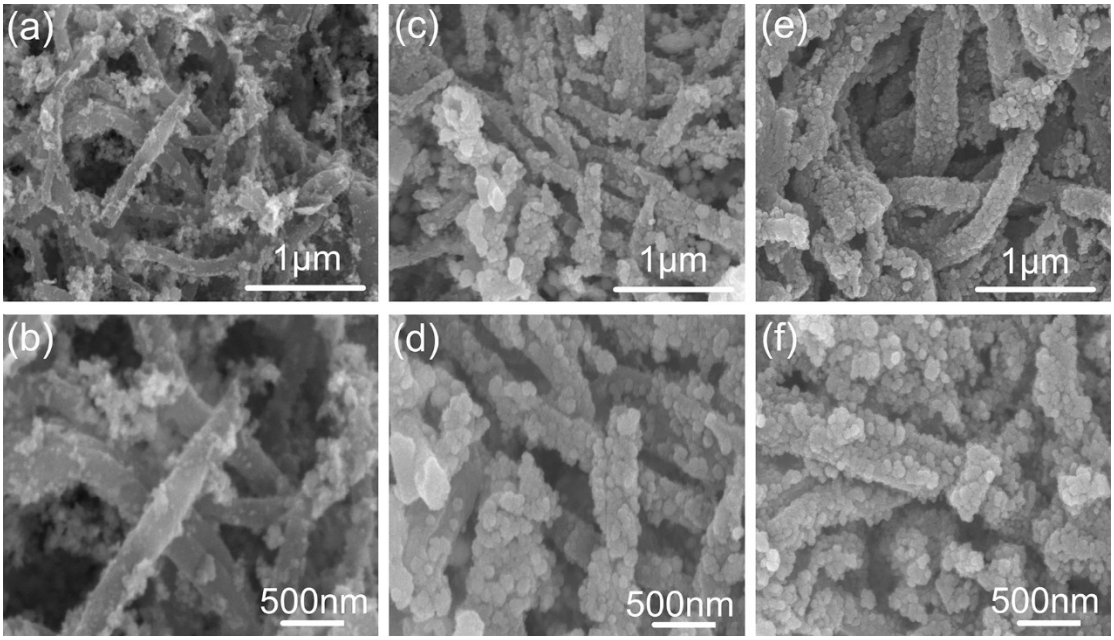

Fig. S3 SEM images of (a,b) Co/CNFs-450, (c,d) Co/CNFs-550 and (e,f) Co/CNFs-650 interlayer.

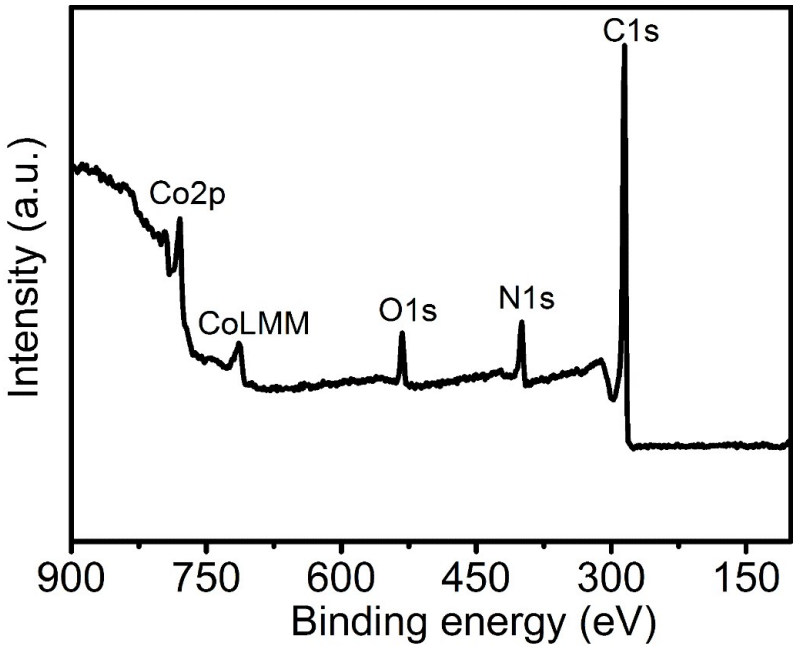

Fig. S4 The XPS spectra of the Co/CNFs-750.

X-ray photoelectron spectroscopy (XPS) analyses were performed to exhibit the surface chemical composition of the Co/CNFs-750. As shown in the Fig. S4, the sharp peaks at 781.27, 533.94, 400.66 and 284.61 eV correspond to Co2p, O1s, N1s and C1s, respectively, indicating the existence of cobalt, oxygen, nitrogen and carbon elements in the Co/CNFs-750.

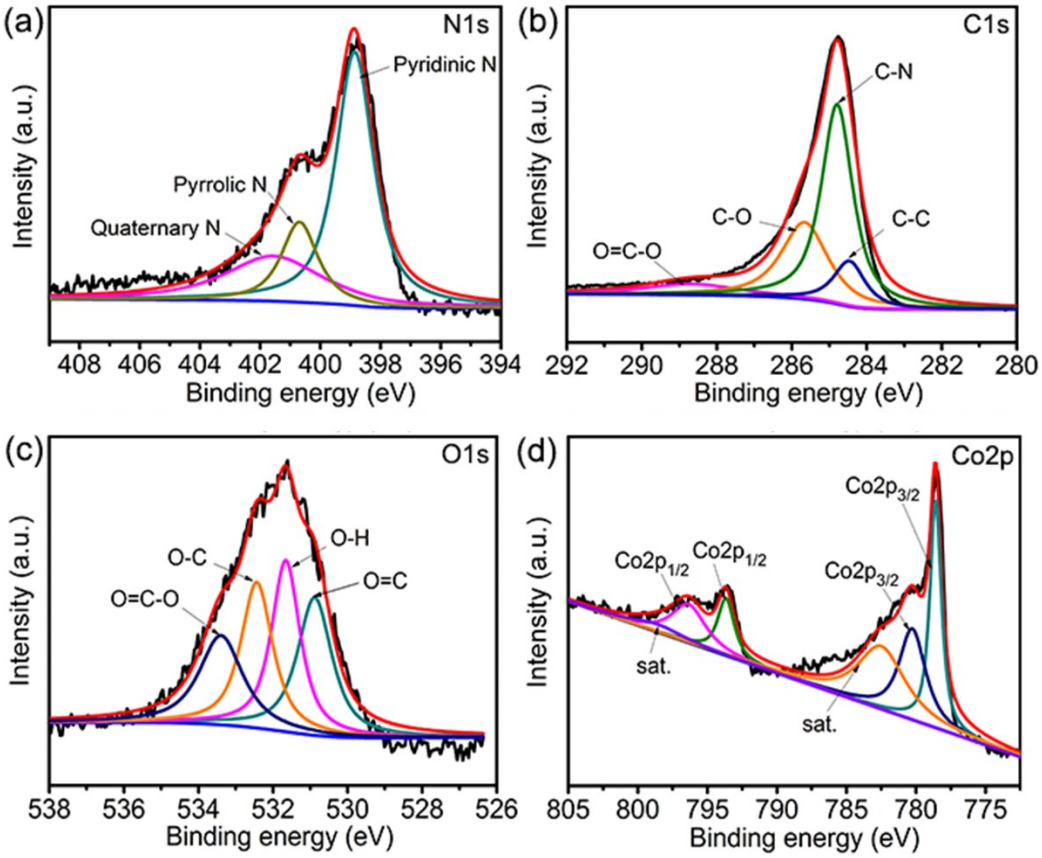

Fig. S5 XPS spectra of the Co/CNFs-750: (a) N1s spectrum, and (b) C1s spectrum, and (c) O1s spectrum, and (d) Co2p spectrum.

The N1s spectrum in Fig. S5a could be fitted to three peaks at 401.70, 400.68, and 398.87 eV, correspond to quaternary N, pyrrolic N and pyridinic N, respectively.[1-2] These N-containing functional groups would be propitious to guide Li nucleation.[3] Four peaks in Fig. S5b at 288.68, 285.65, 284.78 and 284.45 eV corresponding to O=C-O, C=O, C-N and C-C were observed in the C1s spectrum. The existence of C-N bond confirmed that N atoms have been doped into the graphitic domains.[4-5] It was well known that N-doped carbon materials usually displayed impressive properties such as enhanced electrical conductivity and catalytic activity.[5] For the

O1s (Fig. S5c), the spectrum can be divided into four peaks at 533.37, 532.44, 531.67, 530.88 eV, corresponding to the binding states of O=C-O, O-C, O-H and O=C, respectively.[6-7] The high-resolution Co2p XPS spectrum (Fig. S5d) was divided into two spin-orbit doublets. The first doublet was located at 778.58 eV and 793.65 eV, corresponding to the $Co2p_{3/2}$ and $Co2p_{1/2}$ of metallic Co (0),[8-9] and the second doublet was located at 780.25 eV and 796.34 eV, corresponding to $Co2p_{3/2}$ and $Co2p_{1/2}$ of Co-N_x.[9-10]

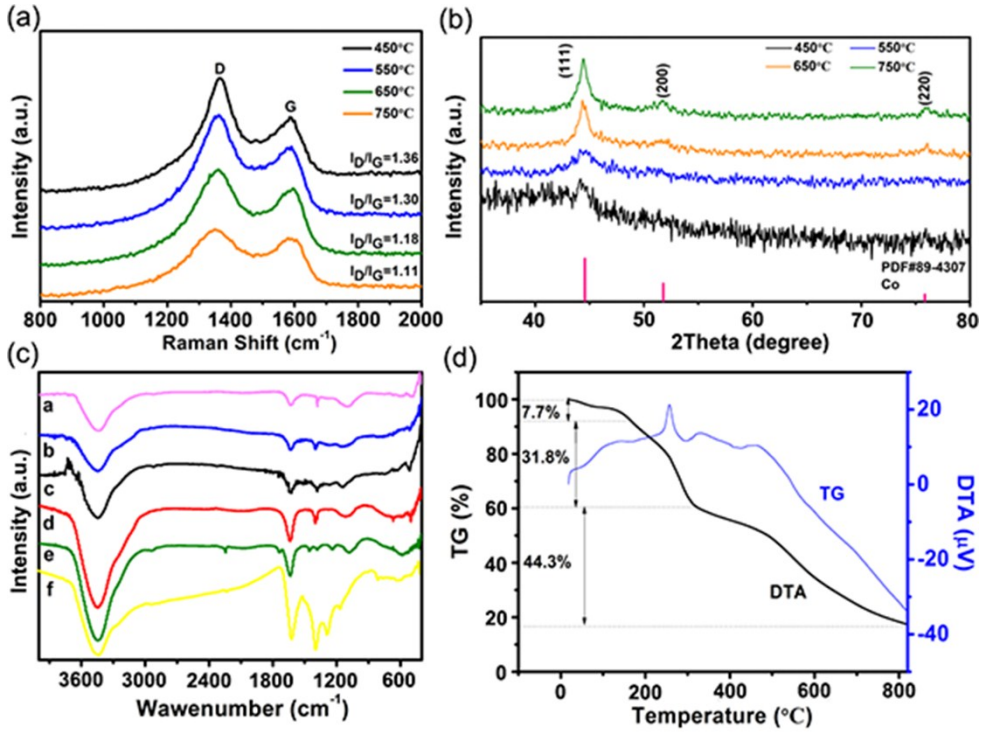

Fig. S6 (a) Raman spectra, and (b) XRD spectra of the Co/CNFs in different calcination temperature at 450 ℃, 550 ℃, 650 ℃, 750 ℃, respectively. (c) The FTIR spectrum: the spectra of the Co/CNFs in the calcination temperature at 450 ℃ a, 550 ℃ b, 650 ℃ c, 750 ℃ d, the spectra of pure PAN fibers before calcination e, the spectra of pure PAN fibers after calcination f. (d) TG spectra of the purple ZIF-67 crystals on PAN NFs film at N_2 atmosphere.

To identify the degree of graphitization in Co/CNFs, Raman spectra (Fig. S6a) was conducted. Generally speaking, the band at 1358 cm^{-1} originated from sp^3-hybridized carbon (D-band) while the band at 1585 cm^{-1} indicated sp^2-hybridized carbons (G-band).[11] The I_D/I_G value which usually provided an index for the crystallinity degree of carbon materials. I_D/I_G value changes from 1.36 to 1.11 with increase of the temperature ranging from 450 to 750 ℃. The result illustrats that the graphitic level increased with the rising of the heat treatment temperature.[12] Moreover, according to the XRD patterns (Fig. S6b). All diffraction peaks could be assigned to the crystalline phase of metallic Co (Joint Committee on Powder Diffraction Standards (JCPDS file no. 89-4307). The three prominent diffraction peaks located at 2θ of 44.22°, 51.53° and 75.86°, which were indexed to (111), (200), (220) of Co.[12] Significantly, there were no diffraction peaks corresponding to the carbon in XRD spectra, indicating that carbon existed with an amorphous state. Besides, the diffraction peaks of metal Co became sharper with the increase of calcination temperature, which indicated that the crystallization of metal Co nanoparticles increased gradually with carbonization temperature. Fourier transform infrared spectrometry (FTIR) was used to explore the component change on the samples. As illustrated in Fig. S6c (e), the spectrum of pure PAN fibers before calcination exhibits typical PAN absorbance peaks: nitrile (C ≡ N) stretching vibrations at 2242.17 cm^{-1}, methylene (CH_2) groups bending vibrations at 1453.24 cm^{-1} and aliphatic C −H bonds around 2936.95 cm^{-1} with a small and weak peak.[13-14] After heat treatment, as seen in the Fig. S6c (f), the nitrile group (C ≡ N) peak completely disappeared, while C = N and C = O double bonds increased at around 1585-1650 cm^{-1} and C-N single bonds increased at 1241.20 cm^{-1}. The main stabilization mechanism can be attributed to the cross-linking reaction of PAN, which is also known as stabilization or cyclization.[15-16] Further, it could be seen that the bands at (C ≡ N) decrease drastically in

intensity, along with conjugated C = N and C - N formed.[17] This elucidated a reduction of nitrile groups induced by intermolecular crosslinking or intramolecular cyclization.[18] Notability, it could be seen that a tiny and weak peak at 517.19 cm^{-1} (Co-O) in Fig. S6c (a,b,c,d), which may be ascribed to the slight oxidation of Co.[19] The remaining peaks at wavelength of 1389.24, 1118.07 and 3444.30 cm^{-1} were contributed to the presence of C-H bending vibrations, C-C stretching vibrations and bending vibrations of absorbed water, respectively. Furthermore, thermal analyses of the ZIFs-67 crystals on nanofibers film in N_2 atmosphere were carried out using TGA methods. In the Fig. S6d, the samples had roughly three stages of thermal weightlessness corresponding to the physical or chemical reactions. The first small weight loss of 7.7 % from ambient temperature to 166 ℃ with a weak broad endothermic peak on DTA curve was corresponded to the evaporation of absorbed water and trapped solvent in the precursor nanofibers. The second weight loss of 31.8 % was associated with complex chemical reactions of dehydrogenation, cyclization, and cross-linking from 166 ℃ to 318 ℃ with a strong narrow endothermic peak on DTA curve. The third weight loss of 44.3 % could be attributed to the decomposition of PAN polymers.

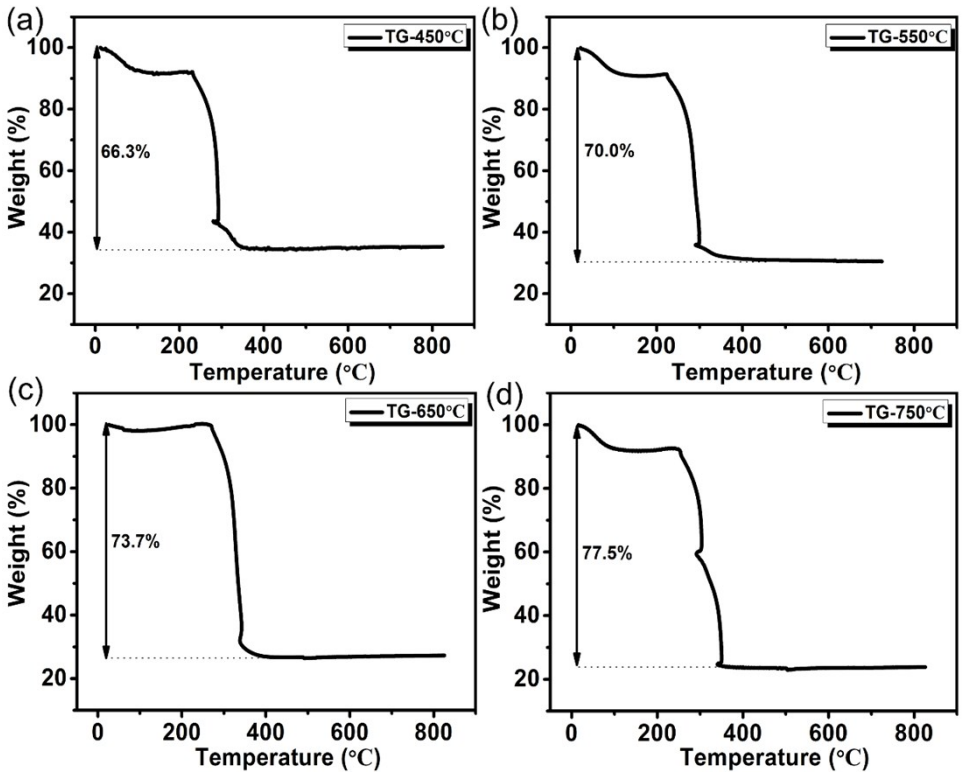

Fig. S7 The weight loss rate of the Co/CNFs in different calcination temperature at (a) 450 ℃, (b) 550 ℃, (c) 650 ℃, and (d) 750 ℃, respectively.

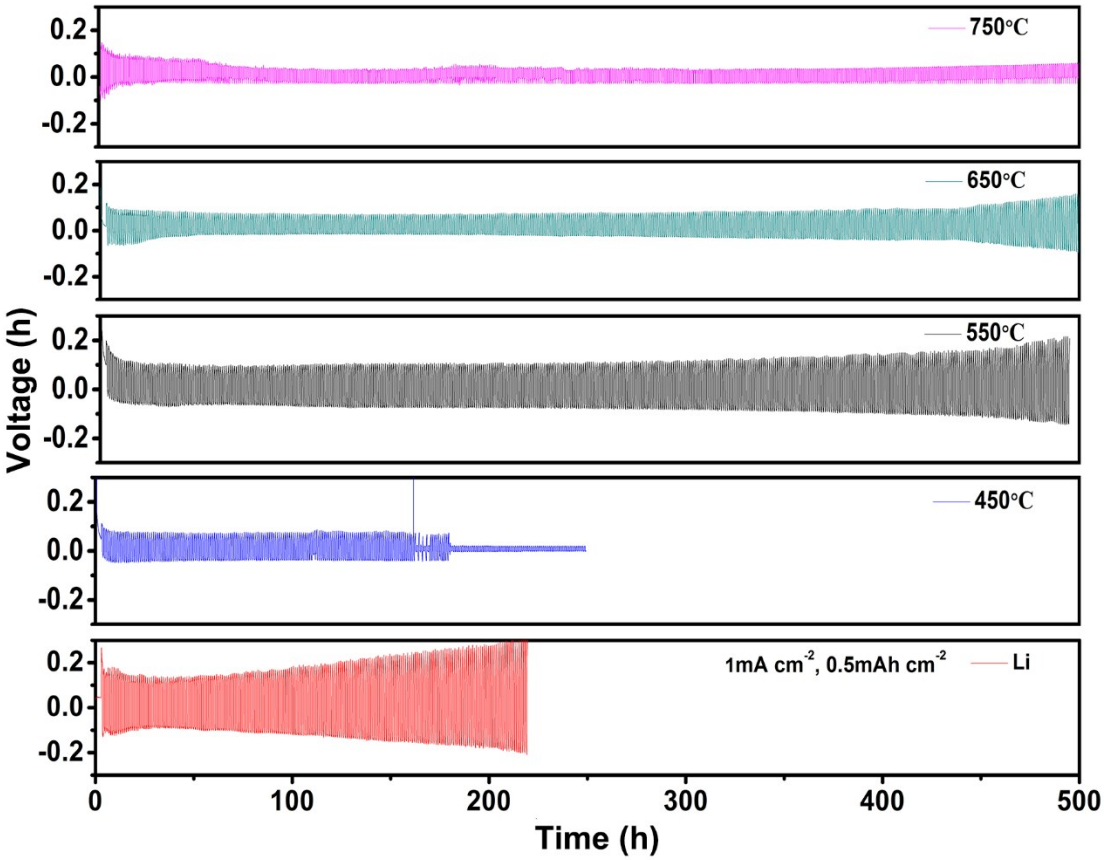

Fig. S8 Voltage profiles of metallic Li plating/stripping in five styles of symmetric cells (Li/Co/CNFs-750 modified Li, Li/Co/CNFs-650 modified Li, Li/Co/CNFs-550 modified Li, Li/Co/CNFs-450 modified Li and Li/Li) at the current density of 1.0 mA cm^{-2} with the capacity limit of 0.5 mAh cm^{-2}.

As shown in Fig. S8, a volatile inconsecutive voltage drop appeared in the cyclic processes of Li/Co/CNFs-450 modified cells, which was attributed to the growth of Li dendrite resulted in the piercing separator during the cycling to cause short-circuit of the batteries. For the Co/CNFs-550 modified Li electrode, the overpotential began to rise after 400 h and climbed to 200.0 mV after 500 h. By contrast, the Co/CNFs-650 modified Li electrode with the lower overvoltage and

the overpotential started to increase after 450 h and rose up to 150.0 mV after 500 h. The phenomenon of the increasing overpotential originated from the large amount of dead Li and severe electrolyte decomposition.

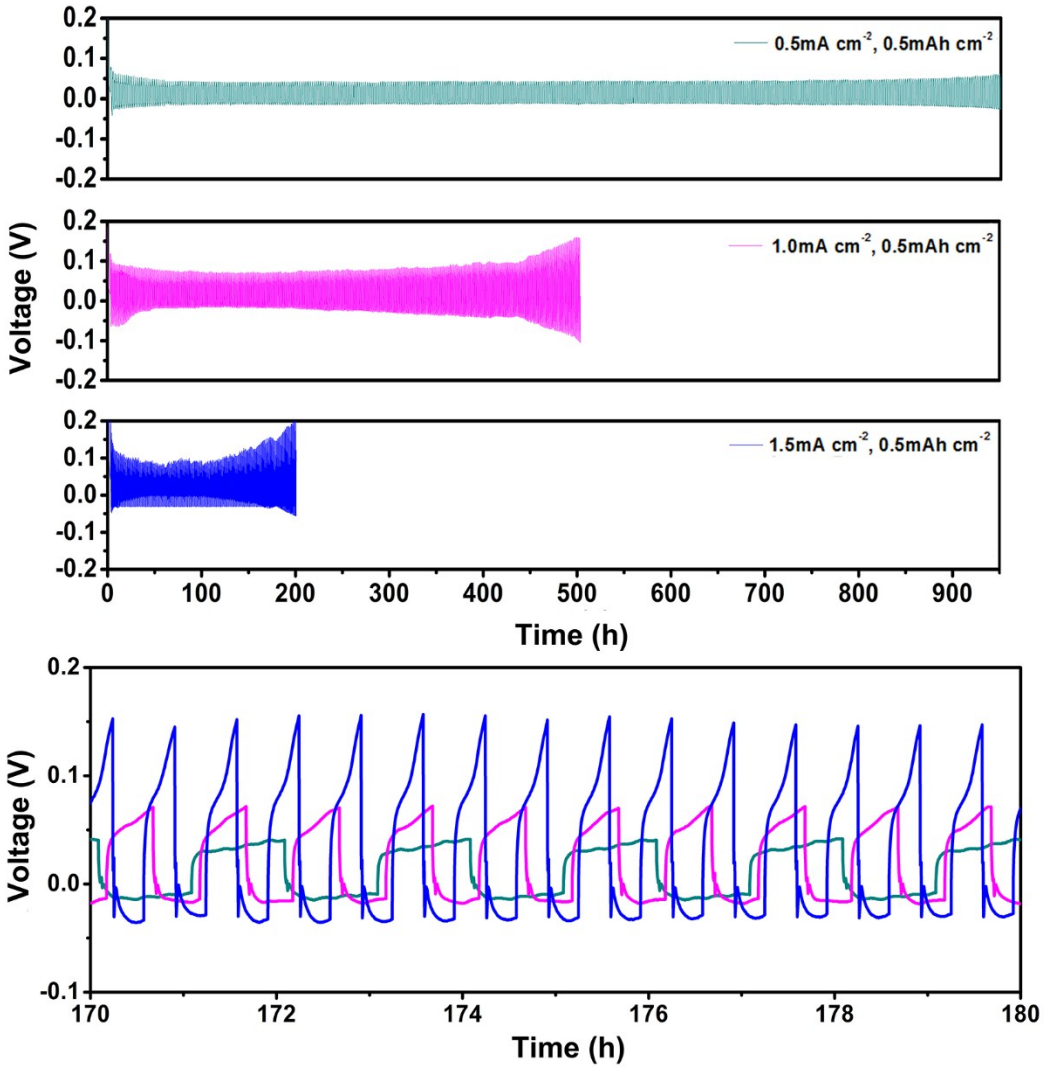

Fig. S9 Voltage profiles of Li plating/stripping in symmetric cells of Li/Co/CNFs-750 modified Li at different current densities of 0.5 mA cm^{-2}, 1.0 mA cm^{-2}, 1.5 mA cm^{-2} with the capacity limit of 0.5 mAh cm^{-2} and its expanded view from 170 to 180 h.

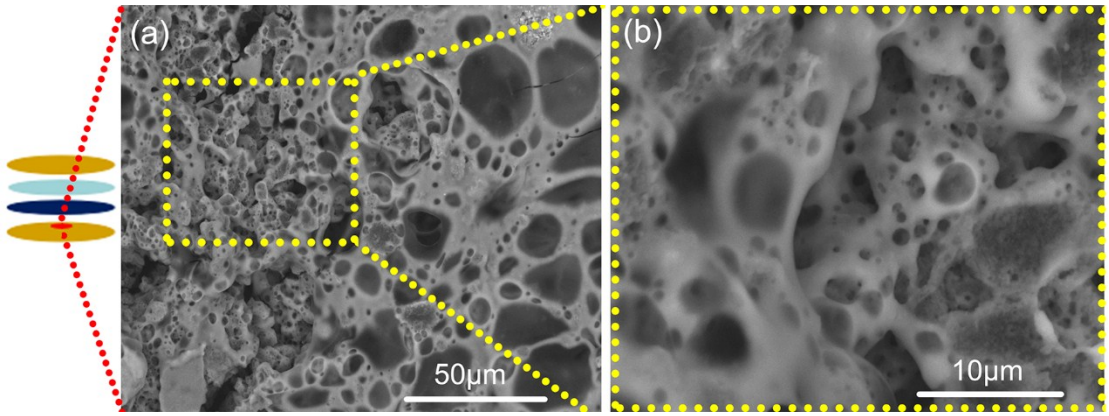

Fig. S10 (a,b) Surface SEM images of the Co/CNFs-750 modified Li electrode at the lithiation capacity of 15 mAh cm^{-2} (30h).

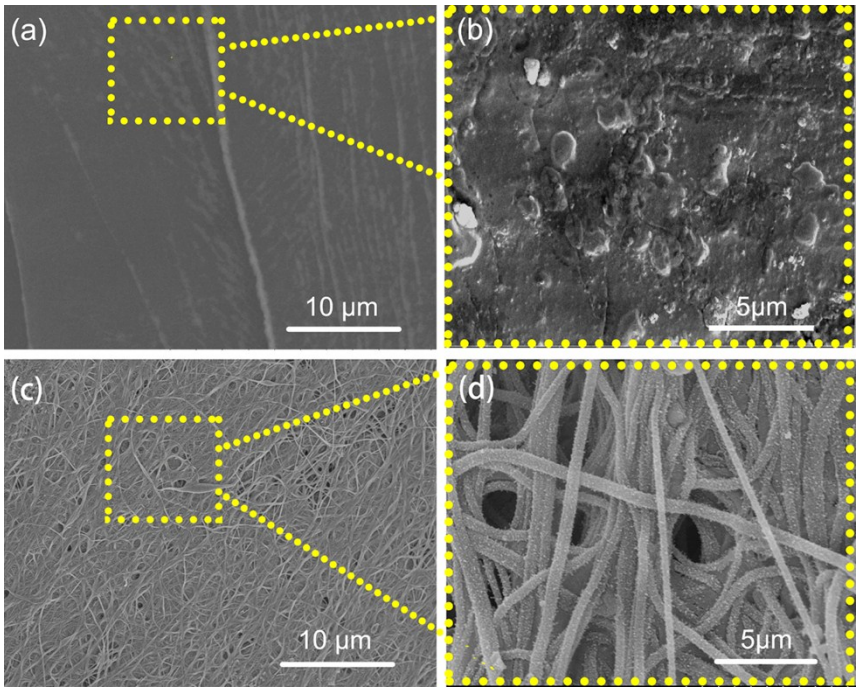

Fig. S11 (a,b) Surface SEM images of the bare Li-metal electrode, and (c,d) the Co/CNFs-750 interlayer before Li deposition.

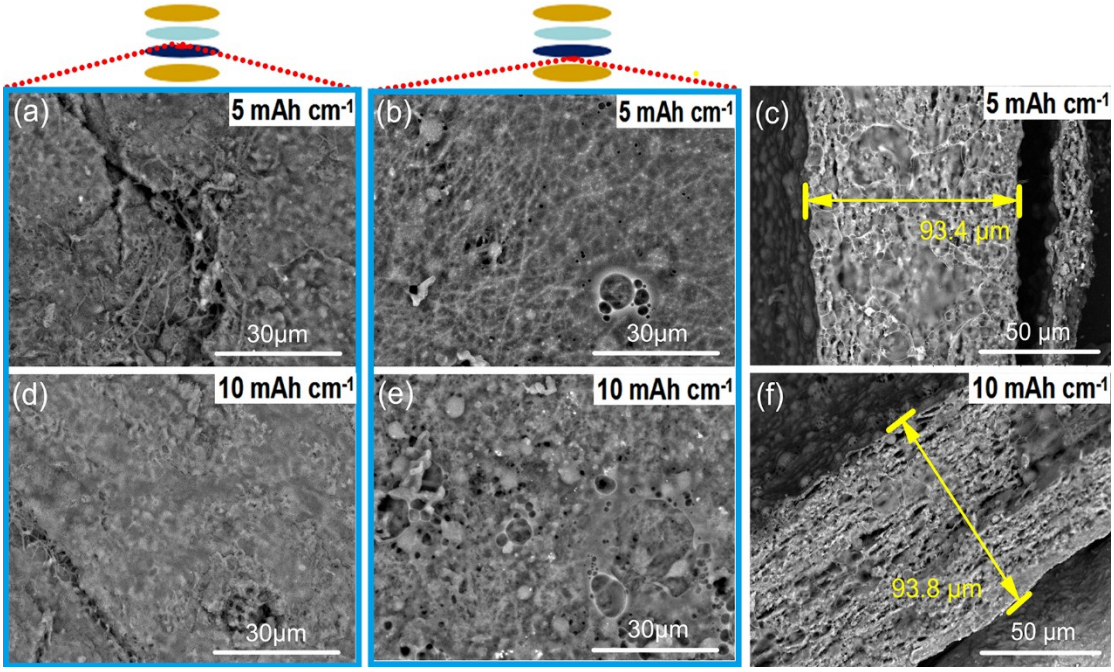

Fig. S12 (a,d) The surface SEM morphologies of the Co/CNFs-750 interlayer facing the separator, and (b,e) the Co/CNFs-750 interlayer backing the separator, and (c,f) the cross-section SEM images of the Co/CNFs-750 interlayer at the different lithiation capacities of 5 mAh cm^{-2} (10 h) and 10 mAh cm^{-2} (20h), respectively.

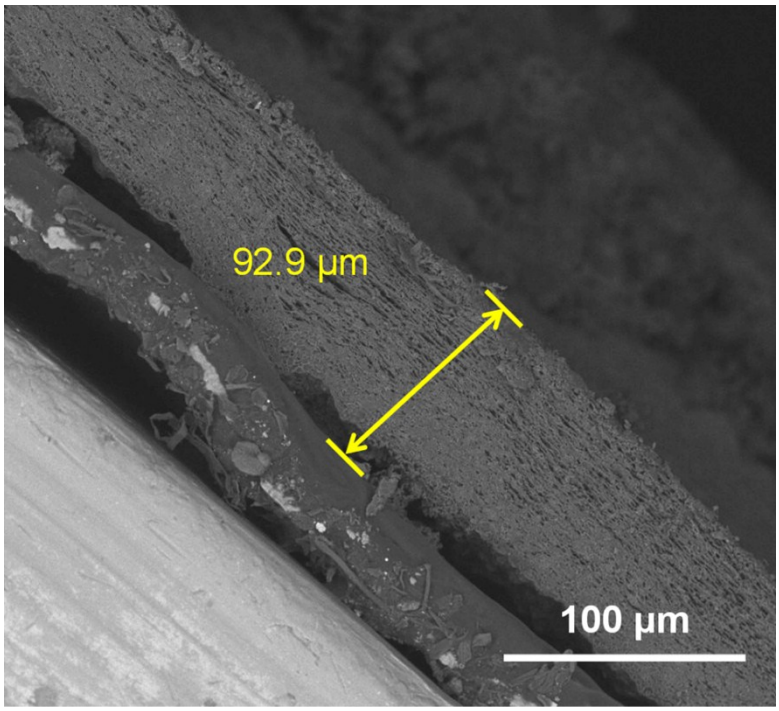

Fig. S13 SEM image of the Co/CNFs interlayers before cycling.

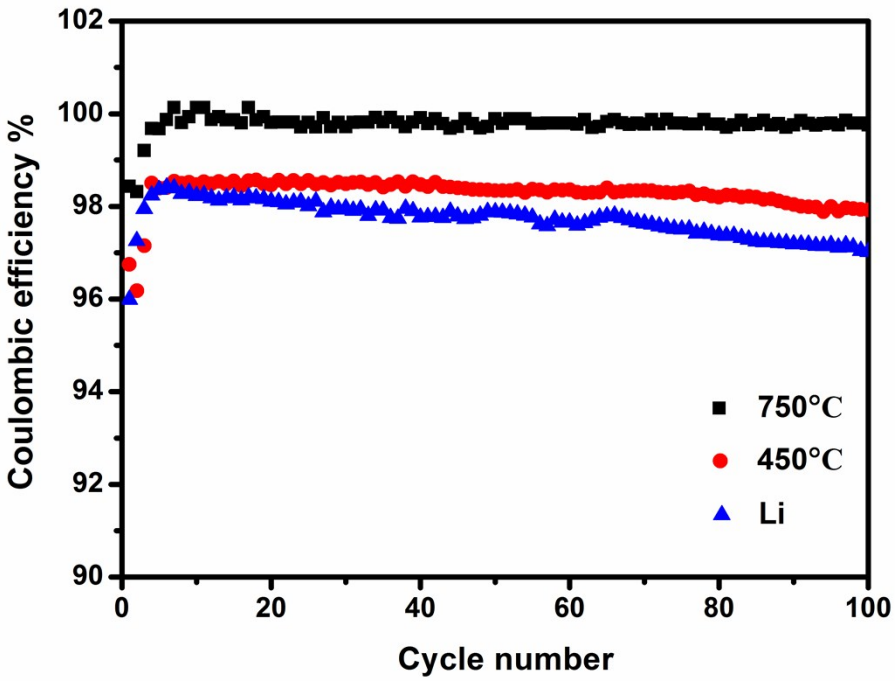

Fig. S14 The coulombic efficiencies of the full cells with three style electrodes at 1.0 C.

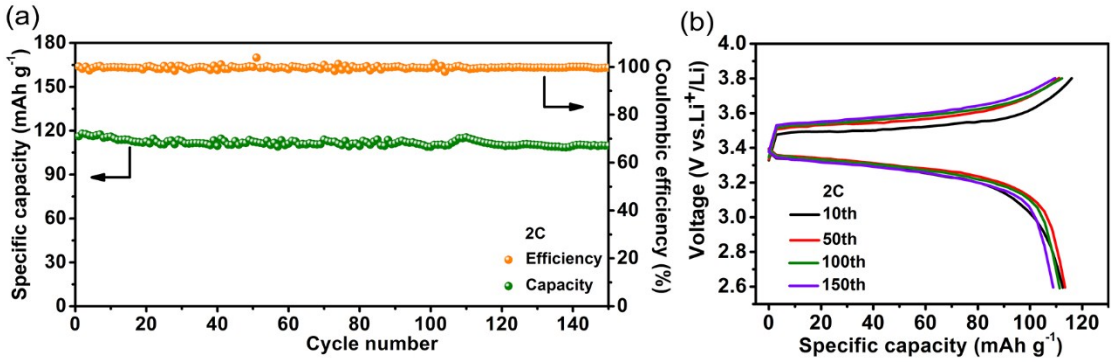

Fig. S15 (a) Cycling performance of the full cells at 2.0 C. (b) The charge/discharge profiles of full cells with $LiFePO_4$ as the cathode and the Co/CNFs-750 modified Li as the anode at 2.0 C.

References

1. K. Xiao, L.-X. Ding, G. Liu, H. Chen, S. Wang and H. Wang, *Adv. Mater.*, 2016, **28**, 5997-6002.

2. L. Liu, Y.-X. Yin, J.-Y. Li, S.-H. Wang, Y.-G. Guo and L.-J. Wan, *Adv. Mater.*, 2018, **30**, 1706216.

3. C. Zhang, L. Fu, N. Liu, M. Liu, Y. Wang and Z. Liu, *Adv. Mater.*, 2011, **23**, 1020-1024.

4. S. Liu, J. Tian, L. Wang, Y. Zhang, X. Qin, Y. Luo, M. A. Abdullah, A.-Y. Abdulrahman and X. Sun, *Adv. Mater.*, 2012, **24**, 2307-2041.

5. A. L. M. Reddy, A. Srivastava, S. R. Gowda, H. Gullapalli, M. Dubey and P. M. Ajayan, *ACS Nano*, 2010, **4**, 6337-6342.

6. B. Li, Y. Xie, C. Wu, Z. Li and J. Zhang, *Mater. Chem. Phys*., 2006, **99**, 479-486.

7. U. Zielke, K. J. Hüttinger and W. P. Hoffman, *Carbon*, 1996, **34**, 983-998.

8. A. Kong, C. Mao, Q. Lin, X. Wei, X. Bu and P. Feng, *Dalton Trans*., 2015, **44**, 6748-6754.

9. J. Wei, Y. Hu, Z. Wu, Y. Liang, S. Leong, B. Kong, X. Zhang, D. Zhao, G. P. Simon and H. Wang, *J. Mater. Chem. A*, 2015, **3**, 16867-16873.

10. Q. Liu and J. Zhang, *CrystEngComm*, 2013, **15**, 5087-5092.

11. S. Abouali, M. A. Garakani, B. Zhang, Z.-L. Xu, E. K. Heidari, J.-Q. Huang, J. Huang and J.-K. Kim, *ACS Appl. Mater. Interfaces*, 2015, **7**, 13503-13511.

12. D. Shin, B. Jeong, B. S. Mun, H. Jeon, H.-J. Shin, J. Baik and J. Lee, *J. Phys. Chem. C*, 2013, **117**, 11619-11624.

13. Y. Aykut, *ACS Appl. Mater. Interfaces*, 2012, **4**, 3405-3415.

14. Y. J. Kim and C. R. Park, *Carbon*, 2005, **43**, 2420-2423.

15. Z. Yue, K. R. Benak, J. Wang, C. L. Mangun and J. Economy, *J. Mater. Chem*., 2005, **15**, 3142-3148.

16. Z. Bashir, *Carbon*, 1991, **29**, 1081-1090.

17. J. Mittal, O. P. Bahl, R. B. Mathur and N. K. Sandle, *Carbon*, 1994, **32**, 1133-1136.

18. W. Zhang, J, Liu and G. Wu, *Carbon*, 2003, **41**, 2805-2812.

19. Y. Lou, J. Liang, Y. Peng and J. Chen, *Phys. Chem. Chem. Phys*., 2015, **17**, 8885-8893.